

7 February 2023

## ERRATA | CORRIGENDA

<http://electronicmaterials.usask.ca/corrigenda/>

Only important scientific content related errors are listed.

**First printing (April 2017)**

**Corrections to print version; the e-version is likely to be correct**

**Page 143:** Figure 2.8. The low temperature residual resistivity value shown is  $7 \times 10^{-5} \text{ n}\Omega \text{ m}$ . This should be  $4 \times 10^{-4} \text{ n}\Omega \text{ m}$ . The  $\rho$  vs  $T$  behavior curves at a higher  $\rho_R$ .

**Page 230:** The wavelength 0.0367 nm in Fig. 3.14(b) and 0.0357 nm in the caption should be 0.0123 nm.

**Page 245:** Equation [3.37], delete the term " $(2m_e/h^2)$ " before " $\alpha$ "

**Page 252:** Photo on bottom right corner of page, caption should read "An STM image of a silicon crystal surface".

**Page 514:** Question 5.15, Figure 5.56. "Ga should have 3 electrons and As should have 5 electrons". (This is correct in the 3rd Edition)

**Page 555:** Last sentence.  $V_r^{-1/2}$  should be  $V_r^{-1/3}$

**Page 556:** Equation 6.30, next equation and p557, the equation starting with "slope =", should have  $N_d$  in the denominator. All calculations and conclusions are correct. (A typographic error only.)

**Page 816:** "decreases" in line 3 below Fig. 8.46 should be "increases" and "increases" in the next line should be "decreases".

Corrected pages 143, 230, 245 and 555-557  
are attached for information

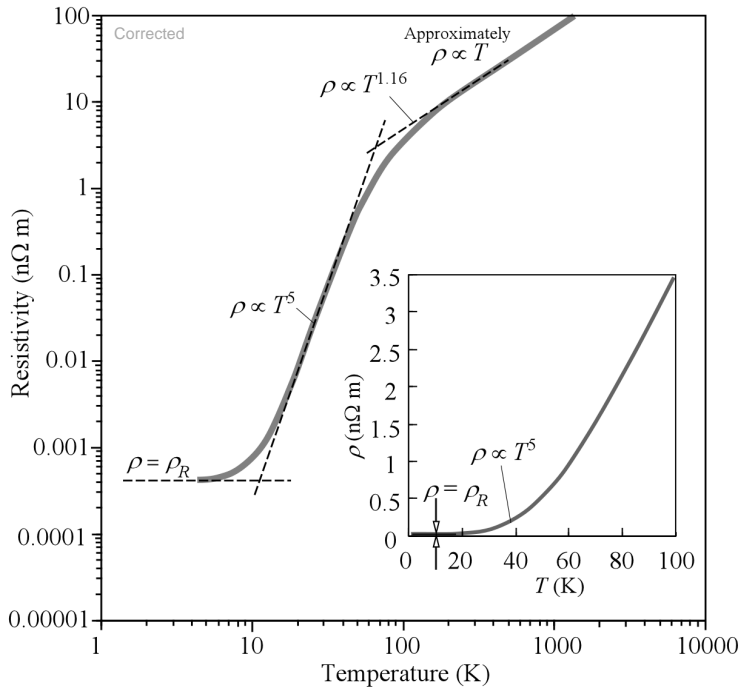


**Figure 2.8** The resistivity of copper from lowest to highest temperatures (near melting temperature, 1358 K) on a log-log plot.

Above about 100 K,  $\rho \propto T^{1.16}$  (approximately  $\rho \propto T$ ), whereas at low temperatures,  $\rho \propto T^5$ , and at the lowest temperatures  $\rho$  approaches the residual resistivity  $\rho_R$ . The inset shows the  $\rho$  versus  $T$  behavior below 100 K on a linear plot. ( $\rho_R$  is too small on this scale.)

Matthiessen's rule, the resistivity becomes  $\rho = DT^5 + \rho_R$ , where  $D$  is a constant. Since the slope of  $\rho$  versus  $T$  is  $d\rho/dT = 5DT^4$ , which tends to zero as  $T$  becomes small, we have  $\rho$  curving toward  $\rho_R$  as  $T$  decreases toward 0 K. This is borne out by experiments, as shown in Figure 2.8 for copper. Therefore, at the lowest temperatures of interest, the resistivity is limited by scattering from impurities and crystal defects.<sup>7</sup>

**MATTHIESSEN'S RULE** Explain the typical resistivity versus temperature behavior of annealed and cold-worked (deformed) copper containing various amounts of Ni as shown in Figure 2.9.

**EXAMPLE 2.7**

**SOLUTION**

When small amounts of nickel are added to copper, the resistivity increases by virtue of Matthiessen's rule,  $\rho = \rho_T + \rho_R + \rho_I$ , where  $\rho_T$  is the resistivity due to scattering from thermal vibrations;  $\rho_R$  is the residual resistivity of the copper crystal due to scattering from crystal defects, dislocations, trace impurities, etc.; and  $\rho_I$  is the resistivity arising from Ni addition

<sup>7</sup> At sufficiently low temperatures (typically, below 10–20 K for many metals and below ~135 K for certain ceramics) certain materials exhibit superconductivity in which the resistivity vanishes ( $\rho = 0$ ), even in the presence of impurities and crystal defects. Superconductivity and its quantum mechanical origin will be explained in Chapter 8.

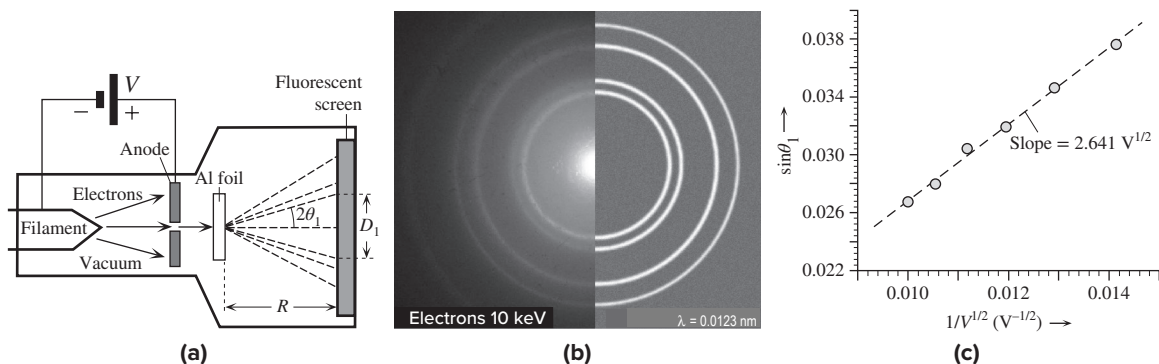


**Figure 3.14** Electron diffraction experiments. (a) A simplified view of an electron diffraction experiment. The voltage  $V$  on the anode accelerates the electrons, which pass the anode toward a fluorescent screen. When the beam impinges on the Al sheet, it becomes diffracted. (b) A comparison of an actual electron diffraction ring pattern from an Al sample (left) with the diffraction pattern that would be obtained from an X-ray beam of wavelength  $0.0123$  nm (right). The electron kinetic energy was  $10$  keV, which corresponds to the same wavelength. (c) A plot of  $\sin \theta_1$  along the  $y$ -axis against  $1/V^{1/2}$  along  $x$ -axis. The best straight line is  $y = 2.641x + 3 \times 10^{-4}$  with an  $R^2$  fit of  $0.9958$ . The experiments confirm the de Broglie relationship,  $\lambda = h/p$ .

† (b) Photo by S. Kasap.

**Table 3.1** Results from electron diffraction experiments on a polycrystalline Al sample

$V$ (kV)	10	9	8	7	6	5
$D_1$ (mm)	19.6	20.5	22.3	23.4	25.4	27.6
$1/V^{1/2}$ ( $V^{-1/2}$ )	0.0100	0.0105	0.0112	0.0120	0.0129	0.0141
$2\theta_1 = \arctan(\frac{1}{2}D_1/R)$	$3.0654^\circ$	$3.2058^\circ$	$3.4867^\circ$	$3.6582^\circ$	$3.9699^\circ$	$4.3125^\circ$
$\sin \theta_1$	0.0267	0.0280	0.0304	0.0319	0.0346	0.0376

*Electron wavelength and anode voltage*

If de Broglie's hypothesis is correct, then the electron's wavelength  $\lambda$  is given by

$$\lambda = \frac{h}{p} = \frac{h}{(2em_e V)^{1/2}} \quad [3.16]$$

When we adjust the anode voltage  $V$ , we are actually changing the de Broglie wavelength  $\lambda$  of the electrons in the experiment. We should be able to use the experimental data to show that this expression is indeed correct and find an experimental value for  $h$  from electron diffraction experiments. The separation  $d$  between the (111) planes in the FCC crystal is<sup>6</sup>  $d = a/3^{1/2}$  where  $a$  is the unit cell lattice parameter, given as  $0.4049$  nm. The first diffraction ring satisfies the Bragg diffraction condition  $2d \sin \theta_1 = n\lambda$  in Equation 3.3, in which  $2\theta_1$  is the diffraction angle, and normally  $n = 1$ . Thus, using Equation 3.15 in the Bragg diffraction condition for the (111) planes

$$\sin \theta_1 = \frac{3^{1/2}\lambda}{2a} = \left[ \frac{3^{1/2}h}{2a(2em_e)^{1/2}} \right] \frac{1}{V^{1/2}} \quad [3.17]$$

If we were to plot  $\sin \theta_1$  versus  $1/V^{1/2}$ , we should get a straight line through the origin whose slope would give us an experimental value for  $h$ . We can find  $\sin \theta_1$  as follows. We

*Bragg condition for the first diffraction ring*

<sup>6</sup> It is not difficult to show that for all cubic crystals, the separation between ( $hkl$ ) planes is given by  $d = a/(h^2 + k^2 + l^2)^{1/2}$ . See Appendix A and Chapter 1.

condition that  $d\psi/dx$  should be continuous (see Figure 3.15). However, the infinite PE well is an exceptional case because  $V = \infty$  means that only  $\psi = 0$  outside the well can satisfy the Schrödinger equation.

We can divide the problem into three regions I, II, and III as shown in Figure 3.17a. In region II, inside the well  $V = 0$ , and we define  $k$  as before

$$k^2 = \frac{2m_e E}{\hbar^2} \quad [3.33] \quad \text{Definition of } k$$

so that in II, the Schrödinger equation becomes

$$\frac{d^2\psi}{dx^2} + k^2\psi = 0 \quad [3.34] \quad \text{Schrödinger equation inside the well}$$

The general solutions to Equation 3.34 is

$$\psi_{\text{II}}(x) = B_1 \exp(jkx) + B_2 \exp(-jkx) \quad [3.35] \quad \text{Electron wavefunction}$$

where  $B_1$  and  $B_2$  are the integration constants we need to find from boundary conditions.

In I and III, the PE is finite and  $V = V_o$  for  $x \leq a$  and  $x \geq a$ . We define

$$\alpha^2 = \frac{2m_e(V_o - E)}{\hbar^2} \quad [3.36] \quad \text{Characteristic well parameter}$$

which depends on  $V_o$ ; and hence  $\alpha$  is a characteristic parameter for the finite well. With the above definition, the Schrödinger equation in I and III becomes<sup>11</sup>

$$\frac{d^2\psi}{dx^2} - \alpha^2\psi = 0 \quad [3.37] \quad \text{Schrödinger equation outside the well}$$

Notice that the second term has the opposite sign to Equation 3.34. The general solutions in I and III are

$$\psi_{\text{I}}(x) = A_1 \exp(\alpha x) + A_2 \exp(-\alpha x) \quad [3.38a] \quad \text{Electron wavefunction in the barrier}$$

$$\psi_{\text{III}}(x) = C_1 \exp(\alpha x) + C_2 \exp(-\alpha x) \quad [3.38b]$$

where  $A$ s and  $C$ s are integration constants.

We are looking for electron energies inside the well, that is,  $E < V_o$ , which means  $\alpha$  is positive. Each of Equations 3.35 and 3.38a, and 3.38b has two constants that we need to find through boundary conditions and requirements on the wavefunction. In the present case,  $\psi(x)$  cannot be zero at the boundaries,  $\psi(x)$  exists both inside and outside the well, and it must be continuous, single valued and have a continuous slope, that is  $d\psi/dx$  must be continuous. (See Figure 3.15.) Further, the normalization requirement means that if we integrate  $|\psi(x)|^2$  over all space, it should be 1, so that  $A_2$  and  $C_1$  must be zero; otherwise  $C_1 \exp(\alpha x)$  would increase to infinity as  $x \rightarrow +\infty$  and similarly so would  $A_2 \exp(-\alpha x)$  as  $x \rightarrow -\infty$ .

Figure 3.17b and c show the wavefunctions and the energies of the electron derived by continuing the mathematical steps above further. Within the well, we have

<sup>11</sup> It is easy to show that while we need an  $\exp(\pm jkx)$  type of solution for Equation 3.34, for Equation 3.37, which has the opposite sign, the solution cannot have the  $j$ , and must be of the form  $\exp(\pm \alpha x)$ .

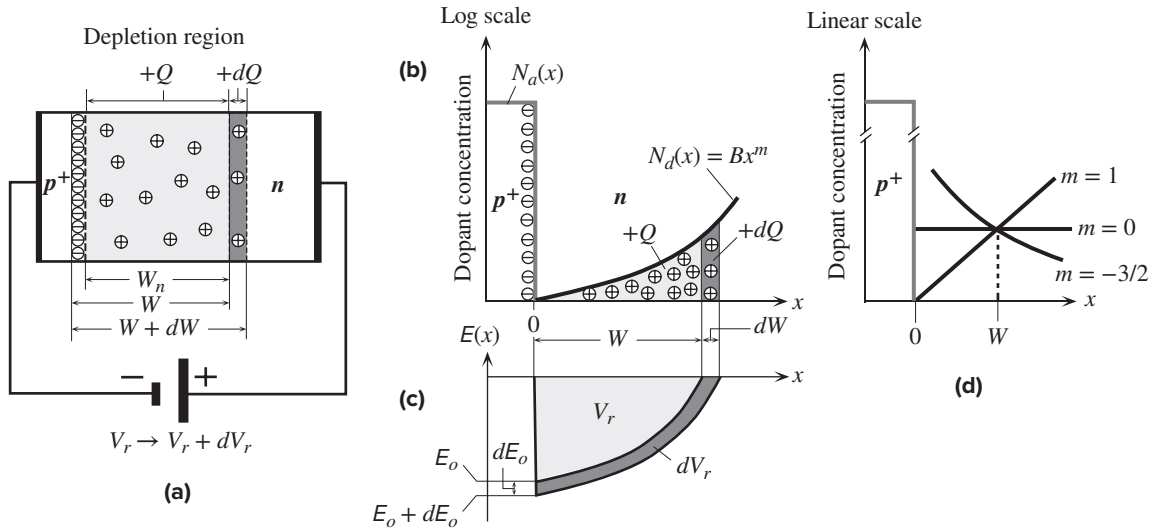


**Figure 6.13** (a) A one-sided  $p^+n$  junction under reverse bias  $V_r$  in which  $W_n \gg W_p$  and  $W \approx W_n$ . The  $n$ -side depletion region has exposed positive donors with total charge  $+Q$ . When  $V_r$  increased by  $dV_r$ ,  $+Q$  increases by  $+dQ$ . There is also an increase in the negative charge by the same amount in the  $p^+$ -side depletion region but this is not shown since it is very narrow. (b) An arbitrary donor concentration  $N_d(x)$  on the  $n$ -side and the regions of  $+Q$  and  $+dQ$  corresponding to  $V_r$  and  $dV_r$ . (c) The field is almost totally on the  $n$ -side, maximum at the metallurgical junction at  $x = 0$ , and falls rapidly into the  $p^+$ -side. The area under the electric field  $|E(x)|$  is the voltage across the depletion region. (d) Shapes of the donor concentration  $N_d(x) = Bx^m$  profiles for  $m = 0$  (abrupt), 1 (linear), and  $-3/2$  (hyperabrupt).

that is

$$C_{\text{dep}} = \frac{\epsilon A}{W} \quad [6.28]$$

General  
depletion  
layer  
capacitance

Equation 6.28 is generally valid even if we do not have a one-sided junction, and is basically Equation 6.27 for a uniformly doped abrupt junction. Since  $W$  depends on the voltage, so does the depletion capacitance.

Suppose that we assume that the donor concentration in the  $p^+n$  junction follows  $N_d(x) = Bx^m$  as shown in Figure 6.13b; and d for three  $m$  values. Obviously,  $m = 0$  is the abrupt junction case. If we integrate  $\rho_{\text{net}} = eBx^m$  across the depletion region  $W$ , we would get the field and if we integrate it again, we would find the total voltage across the depletion region,  $V_o - V$  or  $V_o + V_r$  as a function of  $W$ , that is the dependence of  $W$  on  $(V_o - V)$ . We can then substitute for  $W$  in Equation 6.28 and find  $C_{\text{dep}}$  as

$$C_{\text{dep}} = A \left[ \frac{e\epsilon^{m+1} B}{(m+2)(V_o - V)} \right]^{1/(m+2)} \quad [6.29]$$

General  
depletion  
layer  
capacitance

in which  $V = -V_r$  for reverse bias. Clearly under suitable reverse bias  $V_r > V_o$ , and  $C_{\text{dep}} \propto V_r^{-1/(m+2)}$  which implies that we should design a  $pn$  junction whose  $C_{\text{dep}}$  dependence on the external  $V_r$  can be controlled. Notice that  $m = 1$  gives  $C_{\text{dep}} \propto V_r^{-1/3}$  as expected from Equation 6.27. For many  $pn$  junctions, the dopant concentration

on both or on one side can be approximated as a linear variation ( $m = 1$ ) so that  $C_{\text{dep}} \propto V_r^{-1/3}$ .

The voltage dependence of the depletion capacitance is utilized in **varactor diodes (varicaps)**, which are used as voltage-dependent capacitors in tuning circuits. A varactor diode is reverse biased to prevent conduction, and its depletion capacitance is varied by the magnitude of the reverse bias. The resonant frequency of an  $LC$  circuit with a varactor will be

$$f_o = \frac{1}{2\pi\sqrt{LC_{\text{dep}}}} \propto (V_o - V)^{1/2(m+2)}$$

$f_o$  will be linear in  $V_r$  if  $1/(m + 2) = 1$  or  $m = -3/2$ , which is shown in Figure 6.13d.  $pn$  junctions with such or similar sharp dopant profiles are called **hyperabrupt junctions**.<sup>9</sup>

**EXAMPLE 6.7**

**DEPLETION REGION CAPACITANCE** Table 6.2 provides data on the capacitance  $C$  between the terminals of a reverse-biased Si diode at various reverse voltages  $V_r$ . The diode is a single sided  $p^+n$  junction (fabricated by ion implantation) with a circular electrode that is approximately 500  $\mu\text{m}$  in diameter. The stray capacitance or the packaging capacitance between the terminals is estimated to be 0.5–0.7 pF. Find the built-in voltage  $V_o$  and the donor concentration  $N_d$ . What is your conclusion?

**SOLUTION**

Since this a single-sided  $p^+n$  type Si diode, from Equation 6.27, with  $N_a \gg N_d$ , we have

$$C_{\text{dep}} = A \left[ \frac{e\epsilon N_d}{2(V_o - V)} \right]^{1/2} \quad [6.30]$$

and substituting  $V = -V_r$  and rearranging the equation,

$$\frac{1}{C_{\text{dep}}^2} = \frac{2}{A^2 e\epsilon N_d} (V_o + V_r)$$

A plot of  $1/C_{\text{dep}}^2$  against  $V_r$  should be straight line and we can find  $V_o$  and  $N_d$  from the intercept and the slope. However, the measured  $C$  is not exactly  $C_{\text{dep}}$  but  $C_{\text{dep}} + C_s$ , where  $C_s$  is the stray capacitance  $0.6 \pm 0.1$  pF. Table 6.2 shows a third row in which  $1/C_{\text{dep}}^2$  has been calculated from the second row ( $C$ ) by subtracting  $C_s = 0.6$  pF. Figure 6.14 shows the plot of  $1/C_{\text{dep}}^2$  against  $V_r$ , which follows the expected behavior quite well with the best line being

**Table 6.2** Capacitance of a reverse-biased Si  $pn$  junction diode at 23 °C

$V_r$ (V)	0.5	1.0	2.0	4.0	8.0	10	15
$C$ (pF)	42.6	36.4	29.2	22.4	16.6	15.3	12.6
$1/C_{\text{dep}}^2 \times 10^{-4}$ ( $\text{pF}^{-2}$ )	5.67	7.80	12.2	21.04	39.1	46.3	69.4

<sup>9</sup> See Question 6.10 on varactor diodes. The term hyperabrupt is commonly used for doping profiles in which  $m$  is negative, i.e., the donor concentration decreases with  $x$  in Figure 6.13d.

$p^+n$  junction  
depletion  
capacitance

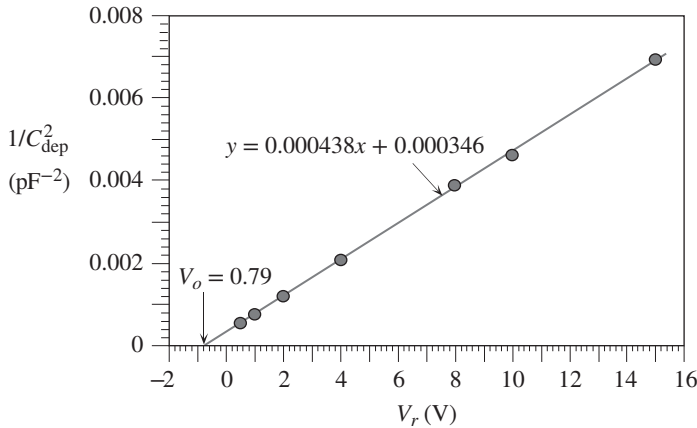


**Figure 6.14** Plot of  $1/C_{\text{dep}}^2$  against  $V_r$  for data in Table 6.2. The solid line is the best fit to the data.

**Table 6.3** Extraction of *pn* junction characteristics from diode capacitance measurements

$C_s$ (pF)	0	0.5	0.6	0.7	1
$V_o$ (V)	0.96	0.82	0.79	0.75	0.67
$N_d$ ( $\text{cm}^{-3}$ )	$7.8 \times 10^{15}$	$7.1 \times 10^{15}$	$7.0 \times 10^{15}$	$6.9 \times 10^{15}$	$6.5 \times 10^{15}$
$N_a$ ( $\text{cm}^{-3}$ )	$3.1 \times 10^{20}$	$1.2 \times 10^{18}$	$4.0 \times 10^{17}$	$8.1 \times 10^{16}$	$4.7 \times 10^{15}$

$y = 0.000438x + 0.000346$  (easily obtained from a graphic software such as Excel). The intercept on the  $V_r$  axis gives  $-V_o$  so that

$$V_o = 0.000346/0.000438 = 0.79 \text{ V.}$$

The slope is

$$\text{Slope} = \frac{2}{A^2 e \epsilon N_d} = 0.000438 \text{ V pF}^{-2},$$

so that substituting  $A = \pi(250 \times 10^{-6} \text{ m})^2 = 1.97 \times 10^{-7} \text{ m}^2$ ,  $\epsilon = \epsilon_o \epsilon_r$ ,  $\epsilon_r = 11.9$ , we find  $N_d = 7.0 \times 10^{21} \text{ m}^{-3}$  or  $N_d = 7.0 \times 10^{15} \text{ cm}^{-3}$ .

We can also extract  $N_a$  by using  $V_o = (kT/e) \ln(N_d N_a / n_i^2)$ , which gives  $N_a = 4.0 \times 10^{23} \text{ m}^{-3}$  or  $4.0 \times 10^{17} \text{ cm}^{-3}$ ; a reasonable value. While these are reasonable values, they do depend on the stray capacitance, especially  $N_a$ . If we repeat the above calculations for different  $C_s$  we would find the results in Table 6.3. Notice that while  $N_d$  values are comparable between different  $C_s$  values,  $N_a$  is extremely sensitive to stray capacitance and varies by five orders of magnitude. Clearly, stray capacitance correction is very important, assuming everything else has been accounted (including the assumption of an abrupt junction).

**LINEARLY GRADED *pn* JUNCTIONS** The simplest way to fabricate a *pn* junction is to diffuse dopants into a Si wafer at a high temperature in a diffusion chamber. Consider an *n*-type Si crystal and we expose one surface of the crystal to a boron gas at a high temperature in a diffusion chamber. B-atoms from the gas enter and diffuse into the Si-crystal as depicted in Figure 6.15. The boron (acceptor) concentration  $N_a$  decays with  $x$  as shown in Figure 6.15 at two times  $t_1$  and  $t_2$  where  $t_2 > t_1$ . The whole acceptor concentration profile  $N_a(x)$  widens

### EXAMPLE 6.8